Physica E: Low-dimensional Systems and Nanostructures 114 (2019) 113627

Contents lists available at ScienceDirect

Physica E: Low-dimensional Systems and Nanostructures

journal homepage: www.elsevier.com/locate/physe

Tunable mirrors and filters in 1D photonic crystals containing polymers

S. Jena*, R.B. Tokas, S. Thakur, D.V. Udupa

Atomic & Molecular Physics Division, Bhabha Atomic Research Centre, Mumbai, 400 085, India

ARTICLE INFO

Keywords:
Photonic crystal
Hydrostatic pressure
Photonic band gap
Mirror
Filter

ABSTRACT

Mechanical tunability of mid-infrared mirrors and filters made of one dimensional photonic crystal (1DPC) containing polymers has been theoretically investigated under hydrostatic compression. The elasto-optic properties of the polymer materials such as poly(methyl-methacrylate) (PMMA) and polystyrene (PS) are considered for tuning the properties of the 1DPCs. Studies on three multilayer 1DPCs viz., PS/SiO_2, PMMA/SiO_2, and PS/PMMA under varying hydrostatic pressures are presented in this paper. The calculation shows that the photonic band gap (PBG) of all the 1DPCs shifts to higher frequency with increasing hydrostatic pressure. The detailed variations in the size of PBG of the mirrors, and operating frequency and full width half maximum of the filters based on all the three 1DPCs have been studied. This study shows that the polymer based 1DPC mirrors and filters can be mechanically tuned, facilitating their applications in designing novel photonic devices.

1. Introduction

Photonic crystals (PC) consist of materials with periodic variation in dielectric constant, which can shape and mould the flow of light inside the crystal [1]. The PC is analogous to solid crystal, in which the motion of electrons is perturbed by the periodic arrangement of lattice atoms. This analogy gives the concept of photonic band structure to describe the dispersion of the light in a PC, exactly like electronic bands in condensed matter physics [2]. The frequency or wavelength ranges in which the propagation of the electromagnetic (EM) wave is forbidden are termed as photonic band gap (PBG) [1,2]. The origin of allowed and forbidden states in the PCs is the Bragg reflection caused by the interference of light reflected by the unit cells of the crystal. The crystal having periodic dielectric permittivity variation in only one direction is called as one dimensional photonic crystal (1DPC) [3]. The introduction of a defect layer in the 1DPC breaks its periodicity, consequently generates allowed states that are strongly localized around the defect in the PBG [4]. The PBG is the high reflection band of mirrors, while the allowed states or defect modes in the PBG creates narrow passband in filters. Moreover, the PBG and the defect mode in a 1DPC have potential applications to design and develop various sensors. Peng et al. [5] have reported 1DPC for refractive index sensing, while Rahmat et al. [6] have reported optical biosensor based on 1DPC with defects. Bouzidi et al. have presented 1DPC as a tiny gas sensor to detect the gas concentration in ambient air [7] and a biosensor for monitoring blood glycemia [8].

Tunable PCs have received considerable attention in recent years, in which the PBG and the defect mode of the PCs are tuned by the external parameters such as electric field [9,10], magnetic field [11,12], temperature [13,14], and pressure [15,16]. In particular, a significant research is being carried out on PC based pressure sensors, in which pressure tunable optical properties of the PC decide the sensitivity of the sensors [17–19]. A. Herrera et al. [20] and F. Segovia et al. [21,22] have reported blueshift of PBG, defect mode, and transmission spectrum of superconductor-semiconductor 1DPCs with increasing hydrostatic pressure. Tefelska et al. [23] have experimentally shown that the PBG of photonic liquid crystal fibres becomes narrow towards longer wavelength with increasing hydrostatic pressure. Wu et al. [24] have reported that the reflection spectrum of PC fibre based Fabry-Perot Interferometer shifts towards shorter wavelength with increasing pressure having sensitivity around 5.8 pm/MPa. Similar experimental demonstration has been reported for a twin-core PC fibre by Liu et al. [25] with increasing pressure from 0 to 45 MPa. The external applied pressure basically changes the dielectric permittivity and/or magnetic permeability of the constituent materials; consequently, varying the PBG as well as the optical properties. The constituent materials can be dielectrics, semiconductors, metals, superconductors etc. Polymer materials can also be used as a constituent material in the PCs for various applications such as reflectors and filters at the THz range [26–28], as well as pressure sensors [29,30], and their properties can be drastically tuned by compressing [31] or stretching [32] the device. Most of the recent theoretical works [20–22,33–35] report the tunable one dimensional photonic crystals at hydrostatic pressures more than 5 GPa. The generation and control of such high pressure pose practical

* Corresponding author.
E-mail addresses: shuvendujena9@gmail.com, shujena@barc.gov.in (S. Jena).

https://doi.org/10.1016/j.physe.2019.113627
Received 5 March 2019; Received in revised form 21 May 2019; Accepted 5 July 2019
Available online 09 July 2019
1386-9477/

challenges with regard to its implementation for experiments and device developments. In the present study, the tunable properties of 1DPC mirrors/filters made of polymer materials have been explored at hydrostatic pressure ≤ 0.2 GPa, which is relatively lower pressure that makes the related experiment relatively easier. The advantage of considering polymer materials is that they exhibit elasto-optic effect [36], whereby optical properties are readily tunable by applying pressure. Here, we have considered two polymer materials of PMMA, and PS as well as fused silica (SiO_2) in the theoretical modelling for designing 1DPC based mirrors and filters. These designs are studied for their elasto-optic properties.

There is a rising interest in the mid-infrared spectral range of 10–100 THz or 3–30 μm, because this region holds strong vibrational signatures for a number of gases and molecules, therefore photonic devices have a potential for various applications in environmental and bio-chemical sensing, defence and security, medicine, thermal imaging, safety monitoring, astronomy, and infrared free-space optical communication [37–39]. A crucial requirement for mid-infrared photonic devices is low loss. The materials PMMA, PS and SiO_2 have excellent transparency in the 10–100 THz range except some narrow absorption peaks in this range [40–42]. The mirrors and filters have been designed for spectral range of 60–65 THz, considering that these materials have no absorption peaks in this range. Similar polymer based photonic devices are also feasible in other frequency ranges within 10–100 THz by varying the size of the unit cell provided that the materials are transparent in that spectral range. In the present work, three multilayer 1DPCs have been considered: PS/SiO_2, PMMA/SiO_2, and PS/PMMA to design mirrors and filters. The photonic band structures and the optical properties of the mirrors and the filters have been investigated with varying hydrostatic pressure to explore their properties of mechanically tunability.

2. Theoretical method and model

2.1. Transfer matrix method

Fig. 1(a) illustrates the design of high reflection mirror in the spectral region of 60–65 THz. The 1DPC consists of the structure $(AB)^{2N}$ with the two materials A and B having refractive index and thickness (n_Ad_A) and (n_Bd_B), respectively. Fig. 1(b) illustrates the design of a narrow bandpass filter in the spectra region 60–65 THz. The necessary allowed states in the PBG for bandpass filter is achieved by inserting defect layer D between the centre of the multilayer $(AB)^{2N}$. The defect layer thickness and refractive index are denoted by (n_Dd_D). The multilayer structure for the filter surrounded by air is $(AB)^{N}D(AB)^{N}$. The

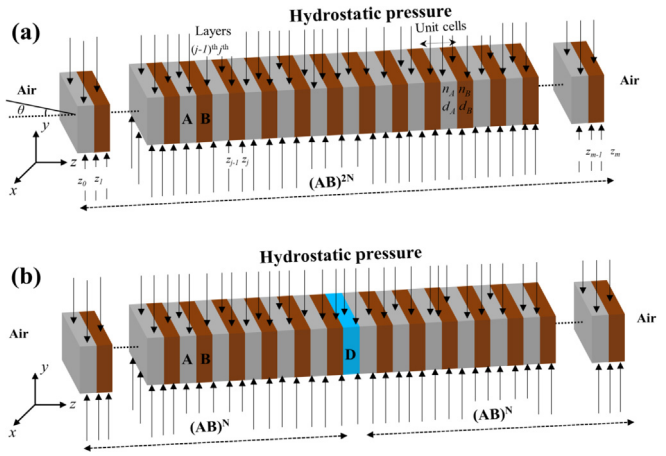

Fig. 1. Schematic of (a) $(AB)^{2N}$ 1DPC (Mirror), and (b) $(AB)^{N}D(AB)^{N}$ defect layer structured 1DPC (Filter) under hydrostatic pressure. D (air) is the defect layer.

spectral transmission of the mirror and the filter is calculated using transfer matrix method (TMM). The layers in the 1DPC are assumed to be homogeneous and isotropic. The layers are considered to be non-magnetic *i.e.* magnetic permeability $\mu = 1$. The electromagnetic (EM) wave is incident normally to the 1DPC and propagates in the z-direction. Using the continuity conditions, the electric and magnetic fields at any two positions z and $z + d_j$ in the jth layer can be related by a transfer matrix [43].

$$M_j(d_j,\omega) = \begin{pmatrix} \cos k_j d_j & \frac{i}{\eta_j}\sin k_j d_j \\ i\eta_j \sin k_j d_j & \cos k_j d_j \end{pmatrix} \quad (1)$$

where d_j (j = A, B, D) is the thickness of the layers, ω is the angular frequency of the incident wave, $k_j = (\omega/c)$ $n_j \cos\theta_j = (\omega/c)n_j\sqrt{1-(\sin^2\theta/n_j^2)}$ is the propagation wave-vector along the z-direction, n_j is refractive index and θ_j is the angle of incidence in the jth layer, θ is the incident angle, and c is the speed of light in vacuum.

Using Snell's law $n_j \sin\theta_j = n_0 \sin\theta$, we obtain $\eta_j = n_j \cos\theta_j = n_j\sqrt{1-(\sin^2\theta/n_j^2)}$ for TE wave, and $\eta_j = \cos\theta_j/n_j = \sqrt{1-(\sin^2\theta/n_j^2)}/n_j$ for TM wave. Since the electric and magnetic field are continuous at layer boundaries, the field can be calculated from its boundary at $z = z_0 = 0$ to $z = z_m$ via the transfer matrix M, also known as the characteristic matrix of the multilayer structure given by

$$M = M_m M_{m-1}.....M_1 = \begin{pmatrix} m_{11} & m_{12} \\ m_{21} & m_{22} \end{pmatrix} \quad (2)$$

For $(AB)^{2N}$ multilayer 1DPC, the total transfer matrix is given by

$$M(\omega) = \begin{pmatrix} m_{11} & m_{12} \\ m_{21} & m_{22} \end{pmatrix} = (M_A M_B)^{2N} \quad (3)$$

By keeping air gap as defect layer (D) in the middle of the 1DPC, the multilayer structure becomes $(AB)^{N}D(AB)^{N,}$ whose total transfer matrix is given by

$$M(\omega) = \begin{pmatrix} m_{11} & m_{12} \\ m_{21} & m_{22} \end{pmatrix} = (M_A M_B)^N M_D (M_A M_B)^N \quad (4)$$

The transmission (T) of the plane EM wave through the multilayer 1DPC is given by Ref. [44].

$$T(\omega) = \frac{\mathrm{Re}(\eta_{ex})}{\mathrm{Re}(\eta_{in})}\left|\frac{2\eta_{in}}{(\eta_{ex}m_{11}+\eta_{in}m_{22})+(\eta_{in}\eta_{ex}m_{12}+m_{21})}\right|^2 \quad (5)$$

Here, the incident and exit medium for the EM wave is air ($n_0 = 1$). Hence the value of η_{ex} and η_{in} at normal incident of the EM wave ($\theta = 0°$) are given by $\eta_{in} = \eta_{ex} = n_0 = 1$for both the TE and TM waves.

The theory for EM wave propagation in a PC is analogous to the theory of motion of electrons in crystalline solids. Using Maxwell equations together with Bloch-Floquet theorem, it is possible to find solutions for the EM wave equations of the PC [45]. For an infinite periodic structure N→∞, the photonic band structure along the principal axis of the 1DPC has been calculated by the following angular frequency-wave vector i.e. ω (k) dispersion relation [3]:

$$\cos kd = \cos k_A d_A \cos k_B d_B - \frac{1}{2}\left(\frac{n_A}{n_B}+\frac{n_B}{n_A}\right)\sin k_A d_A \sin k_B d_B \quad (6)$$

where k is the Bloch wave vector along the z-axis, $d = d_A + d_B$ is the thickness of a period, and d_r, n_r, $k_r = (\omega/c)n_r$ are the thickness, refractive index and wave vector in the layer r, respectively, with r = A and B layers respectively. The solution of kd as a function of frequency ω is the so-called photonic band structure. In the transparent 1DPC, the solution of kd is purely real in the passband, while it is purely imaginary in the PBG. The PBG gets wider with increasing refractive index contrast between the materials A and B i.e. n_A/n_B. Here the target is to tune the PBG by compressing the 1DPC under hydrostatic pressure.

2.3. Pressure dependent refractive index

The polymer materials considered in the present study exhibit good elasto-optic properties, allowing their dielectric permittivity or refractive index in the mid-infrared region to be tunable under hydrostatic compression or expansion. Assuming the layers in the 1DPC are isotropic, elastic, and non-piezoelectric, the change in refractive index tensor **ΔN** of a layer under compression is given by Ref. $\Delta N_{ij} = p_{ijkl}\sigma_{kl}$[46], where p_{ijkl} are the Pockels or elasto-optic tensor components and σ_{kl} are the strain tensor components of the layer. The Pockels tensor for an isotropic layer is given by Ref. [46].

$$p = \begin{pmatrix} p_{11} & p_{12} & p_{12} & 0 & 0 & 0 \\ p_{12} & p_{11} & p_{12} & 0 & 0 & 0 \\ p_{12} & p_{12} & p_{11} & 0 & 0 & 0 \\ 0 & 0 & 0 & \frac{p_{11}-p_{12}}{2} & 0 & 0 \\ 0 & 0 & 0 & 0 & \frac{p_{11}-p_{12}}{2} & 0 \\ 0 & 0 & 0 & 0 & 0 & \frac{p_{11}-p_{12}}{2} \end{pmatrix} \tag{7}$$

The strain tensor of a layer due to mechanical compression "P" perpendicular to the principal axis of the 1DPC is given by Ref. [47].

$$\sigma = \begin{pmatrix} \nu\frac{P}{E} & 0 & 0 \\ 0 & -\frac{P}{E} & 0 \\ 0 & 0 & \nu\frac{P}{E} \end{pmatrix} \tag{8}$$

where E and ν are the Young's modulus and Poisson's ratio of the layer respectively. The applied stress modifies the shape and transversal width of the layer. Consequently, the dipole polarization of the layer gets modified and the relative permittivities of the layer along the principal directions of the 1DPC is given by Ref. [36].

$$\varepsilon_m \simeq \varepsilon_0 - \varepsilon_0^2\lambda_m \tag{9}$$

where $\lambda_m$is the eigen values of the matrix ($p_{ijkl}\sigma_{kl}$) and $\varepsilon_0$is the relative permittivity of the layer without compression. In particular, the relative permittivity of the layer along the principal axis (z-direction) of the 1DPC under hydrostatic pressure (P) is given by Ref. [47].

$$\varepsilon(P) = \varepsilon_0 - \frac{\varepsilon_0^2}{2}[\frac{p_{11}}{E}(\nu+1)\,P + \frac{p_{12}}{E}(3\nu+1)P] \tag{10}$$

where p_{11} and p_{12} are the Pockels co-efficients. The Young's modulus, the Poisson's ratio and the Pockels co-efficients [E; ν; ($p_{11}p_{12}$)] of PMMA, PS and SiO_2 are [3.0303 GPa; 0.37; (0.300, 0.297)], [3.3000 GPa; 0.35; (0.320, 0.310)], and [73.0190 GPa; 0.17; (0.121, 0.270)], respectively [36,47].

The refractive index (n) is obtained from the relative permittivity by the equation $n = \sqrt{\varepsilon}$. The variation of mean refractive index of the materials with hydrostatic pressure in the range of 0–200 MPa is calculated using Eq. (10) and plotted in Fig. 2. It can be seen from Fig. 2 that the refractive index of PS and PMMA decreases with increasing compressive pressure, while the change in refractive index of SiO_2 under pressure is negligible. When a polymer material is compressed, the dielectric polarization increases in the direction of the compression and decreases in the perpendicular direction of the compression (z-axis of the 1DPC). Since refractive index is proportional to the dielectric polarization, the refractive index of the polymer material decreases along the principal axis of the 1DPC with increasing compression. Similarly, when the polymer material is tensed, the dielectric polarization decreases in the direction of tension and increases in the direction perpendicular to the tension. Hence the refractive index of the polymer materials increases along the principal axis (z-axis) of the 1DPC with increasing tension. This indicates that tunable mirrors and filters are possible using polymer materials, where the refractive index can be varied by changing the externally applied hydrostatic pressure, thereby tuning the optical properties of 1DPCs. The present work is however limited to studies with hydrostatic compressions only.

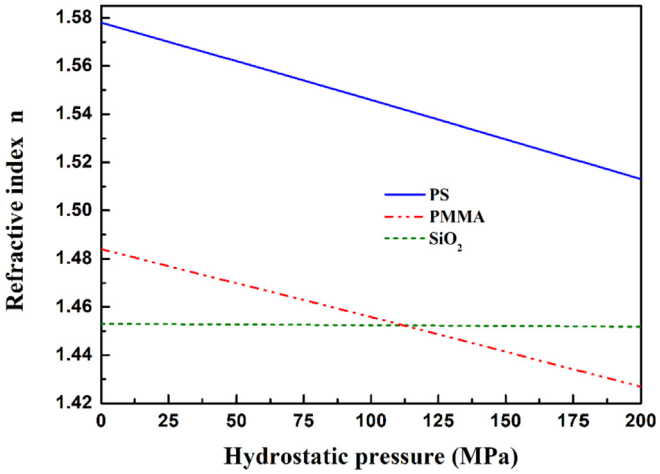

Fig. 2. Variation of refractive index of PS, PMMA, and SiO_2 with hydrostatic pressure.

3. Results and discussion

The combinations of materials, viz. PS/SiO_2, PMMA/SiO_2, and PS/PMMA have been considered for designing 1DPCs based mirrors and filters. Generally, multilayer mirrors used at normal incidence is designed with quarter wave layers *i.e.*$d_A = \lambda_0/4n_A$and $d_B = \lambda_0/4n_B$, where λ_0 is the wavelength of light. The maximum reflection occurs at frequency

$$\omega_0 = \frac{2\pi c}{\lambda_0} = \frac{\pi}{2}\frac{c}{n_A d_A} = \frac{\pi}{2}\frac{c}{n_B d_B} \tag{11}$$

The edges of the high reflection bands are given by$\omega_0 \pm \Delta\omega$ Ref. [48], where

$$\frac{\Delta\omega}{\omega_0} = \frac{2}{\pi}\sin^{-1}(\frac{n_A - n_B}{n_A + n_B}) \tag{12}$$

The thickness of the layers d_A and d_B for different 1DPC based mirrors are calculated using Eq. (11) as per the desired central frequency. The high reflection bandwidth of the mirror depends only on the contrast in refractive index of the two materials. To design narrowband pass filter, air as defect layer is introduced in the middle of two 1DPC mirrors. This defective 1DPC gives resonant transmission at the defect frequency or operating frequency (ω_0) of the filters. The defect layer thickness (d_D) is decided following the resonance condition:

$$(\phi_{AB})_1 + \frac{4\pi n_D d_D}{\lambda_0} + (\phi_{AB})_2 = 2g\pi \tag{13}$$

where g is an integer. For "Air" defect layer ($n_D = 1$), the values $(\phi_{AB})_1 = 0$ and $(\phi_{AB})_2 = \pi$ are the reflection phases at the defect layer/1DPC mirror interfaces. Hence, the minimum thickness of the defect layer for $g = 1$ using Eq. (13) can be expressed as

$$d_D = \frac{\lambda_0}{4} = \frac{2\pi c}{4\omega_0} \tag{14}$$

The defect layer acts as an absentee layer, resulting a narrow transmission window in the middle of the reflection band. The number of AB bilayers (N) for a mirror or filter made of quarter wave thick layers is decided by the reflectivity at normal incidence as [49]:

$$R = [\frac{1 - (n_A/n_B)^{2N}}{1 + (n_A/n_B)^{2N}}]^2 \tag{15}$$

This equation shows that the reflectivity of the mirror increases with increasing number of bilayers. For low refractive index contrast n_A/n_B, larger number of bilayers are required to get high reflectivity as per Eq.

(15). Since the refractive index contrast among the polymer materials and SiO_2 is very low, large bilayer numbers such as N = 25 or 50 have been chosen for different 1DPCs to get maximum reflectivity in the desired spectral region. In addition to this, the strain in the direction normal to the layers (z-axis) is not considered and the size of the unit cell of the 1DPC is assumed to be constant. With these assumptions, the tunable properties of high reflection mirrors and narrow bandpass filters under varying hydrostatic compressive pressure for the three material combinations are discussed below.

3.1. PS/SiO_2 1DPC

In this section, the hydrostatic pressure-dependent photonic band structure and spectral response of the PS/SiO_2 1DPC based mirror and filter are described. Let us first consider the mid-infrared band structure of 1DPC of $(AB)^{2N} = (PS/SiO_2)^{2N}$ embedded in air. For the PS/SiO_2 1DPC mirror, N is fixed at 25, and the stress-free mean refractive index of PS and SiO_2 are denoted by $n_A = 1.578$ and $n_B = 1.453$, respectively in the mid-infrared region [47]. Considering $\omega_0 = 62.5$THz and using Eq. (11), the corresponding thicknesses of PS and SiO_2 are $d_A = 0.76$μm and $d_A = 0.83$μm, respectively. The polymer material PS is less rigid as compared to the dielectric material SiO_2, therefore the refractive index of PS changes significantly with hydrostatic pressure as compared to that of SiO_2, which subsequently affects the PBG of the 1DPC. The calculated photonic band structure of the PS/SiO_2 1DPC under different hydrostatic pressures is plotted in Fig. 3. The PBG occurs between 60.85 and 64.15 THz with bandwidth of 3.3 THz at zero hydrostatic pressure. The figure shows that the both the lower-edge as well as the upper-edge of the PBG undergo blueshift with increasing hydrostatic pressure. It is observed that the shifting of upper-edge is lesser compared to the lower edge with increasing pressure. Ultimately, the bandwidth of the PBG of the PS/SiO_2 1DPC becomes narrow with increasing pressure.

The tunable transmission spectrum of the $(PS/SiO_2)^{50}$ 1DPC high reflection mirror with varying hydrostatic pressure is shown in Fig. 4 (a). The figure shows that high reflection band of the mirror matches exactly with the obtained PBG of the PS/SiO_2 1DPC. The high reflection band-edge blueshifts with increasing hydrostatic pressure. The lower band-edge shifts from 60.85 THz to 63 THz, while the upper band-edge shifts from 64.15 THz to 64.65 THz with increasing pressure from 0 to 200 MPa. The high reflection bandwidth of the mirror is reduced from 3.3 THz at P = 0 MPa to 1.65 THz at P = 200 MPa. These results show that the band-edge as well as bandwidth of the PS/SiO_2 1DPC based high reflection mirrors can be tuned by changing the applied external hydrostatic pressure.

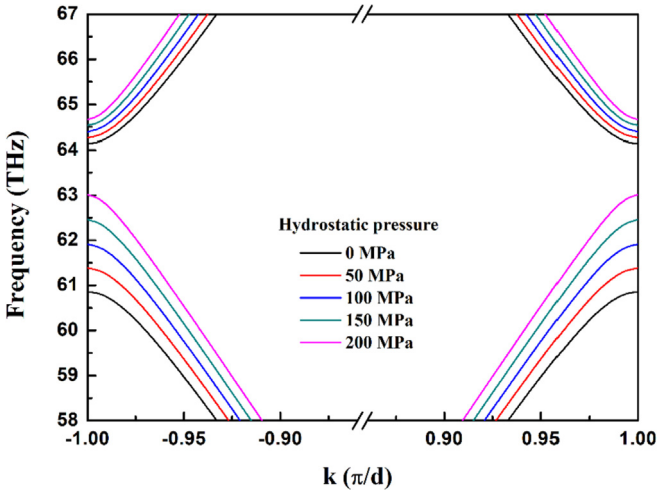

Fig. 3. Photonic band structure of PS/SiO_2 1DPC with varying hydrostatic pressure.

A narrow bandpass filter is designed by introducing air gap as defect layer in the middle of two 1DPCs of $(PS/SiO_2)^{25}$. The thickness of the defect layer as per Eq. (14) is $d_D = 1.2$μm. The photonic structure for the filter is $(PS/SiO_2)^{25}Air(PS/SiO_2)^{25}$. The calculated transmission of the narrow bandpass filter with varying hydrostatic pressure is shown in Fig. 4(b). It is found that the resonant transmission occurs in the photonic band gap and the operating frequency of the filter is significantly changed with varying pressure. The operating frequency blueshifts from 62.5 THz at P = 0 MPa to 64 THz at P = 200 MPa. The full width half maximum of the filter becomes wider with increasing hydrostatic pressure, consequently degrades the quality factor (Q factor) of the filter.

3.2. $PMMA/SiO_2$ 1DPC

We have considered a $(PMMA/SiO_2)^{2N}$ 1DPC embedded in air with N = 50 for getting a good reflection band. The refractive index and the corresponding thickness of PMMA and SiO_2 are taken as ($n_A = 1.484$, $d_A = 0.81$μm) and ($n_B = 1.453$, $d_A = 0.83$μm), respectively. The photonic band dispersion curves of the $PMMA/SiO_2$ 1DPC with varying external hydrostatic pressures are shown in Fig. 5. The PBG shifts to higher frequency with increasing hydrostatic pressure. The lower band-edge shifts from 62.1 THz to 63.4 THz, while the upper band-edge shifts from 62.9 THz to 64.1 THz with increasing pressure from 0 MPa to 200 MPa. It is observed that the size of the PBG decreases with increasing pressure and is almost zero for a pressure of 100 MPa, after which it increases with increasing pressure. This is mainly because the refractive index contrast is zero at ~100 MPa, whereas it is non-zero on either side of the critical pressure. The size of the PBG decreases from 0.8 THz at 0 MPa to 0.05 THz at 100 MPa, whereas it increases to 0.7 THz at 200 MPa. This corresponds to a change of around 60% in PBG of the 1DPC with a pressure variation of 0–100 MPa indicating that external applied pressure can be used to tune the PBG of the $PMMA/SiO_2$ 1DPC from zero to a finite value.

The transmission spectrum of the $(PMMA/SiO_2)^{100}$ with varying hydrostatic pressure is shown in Fig. 6 (a). The 1DPC has high reflection in a very narrowband resulting in a narrow band reflecting mirror. The high reflection band of the mirror matches with the calculated PBG of the $PMMA/SiO_2$ 1DPC. The high reflection band-edges shifts to higher frequency with increasing hydrostatic pressure. The high reflection bandwidth as well as reflectivity of the mirror decreases with increasing pressure up to 100 MPa, where it reaches minima and then both the value increases with further increasing pressure. The high reflection band almost disappears at pressure of 100 MPa following the observed nearly zero-refractive index contrast at this pressure. The study shows that mechanically switchable mirror can be made using the $PMMA/SiO_2$1DPC by varying pressure from 100 MPa on either side of the desired wavelength range, as the transmission can be varied from more than 90% to less than 5% by tuning pressure. It may be mentioned that this effect is similar to the case of electrically switchable mirrors made of liquid-crystal gels [50]. This simulation shows that bandwidth and reflectivity of the mirror can be largely varied from a maximum value to a minimum value by tuning applied hydrostatic pressure for this design of 1DPC mirror.

For narrow bandpass filter, the thickness of defect layer (air gap) as per Eq. (14) is $d_D = 1.2$μm. The structure of the filter is $(PMMA/SiO_2)^{50}Air\ (PMMA/SiO_2)^{50}$. The spectral transmission of the filter is shown in Fig. 6(b) with varying hydrostatic pressure. The figure shows that the passband appears in the centre of the PBG and the operating frequency of the filter shifts to higher frequency with increasing pressure. The operating frequency shifts from 62.5 THz at P = 0 MPa to 63.7 THz at P = 200 MPa. The bandwidth of the filter increases with pressure and the passband almost disappears at pressure of 100 MPa, and then reappears with narrower bandwidth with further increasing pressure. The results show that elastically switchable filter can be made using the $PMMA/SiO_2$ 1DPC. The Q factor of the filter can be

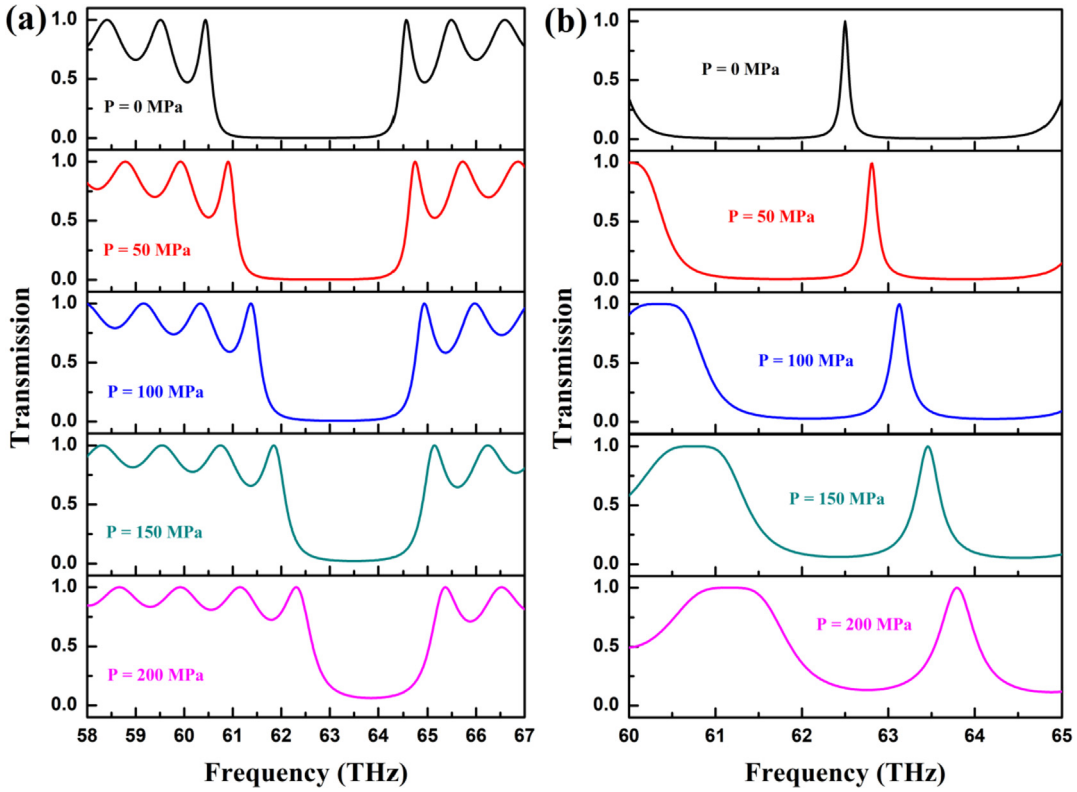

Fig. 4. Transmission spectra of (a) $(PS/SiO_2)^{50}$ 1DPC as high reflection mirror, and (b) $(PS/SiO_2)^{25}Air(PS/SiO_2)^{25}$ 1DPC with defect as narrow bandpass filter with varying hydrostatic pressure P.

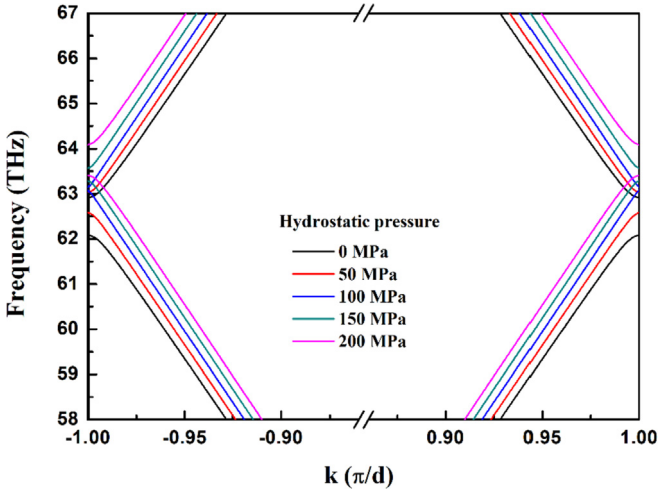

Fig. 5. Photonic band structure of $PMMA/SiO_2$ 1DPC with varying hydrostatic pressure.

significantly tuned by varying applied hydrostatic pressure. The Q factor of the filter can be improved further by increasing the N value to a higher number.

3.3. PS/PMMA 1DPC

Let us consider 1DPC made with the structure of $(PS/PMMA)^{2N}$ 1DPC with N = 25. The alternating layers of PS and PMMA have refractive index and thickness as ($n_A = 1.578$, $d_A = 0.78\,\mu m$) and ($n_B = 1.484$, $d_B = 0.83\,\mu m$), respectively. The computed photonic band structure of the PS/PMMA 1DPC with varying hydrostatic pressure is plotted in Fig. 7. The figure shows that the PBG shifts significantly towards higher frequency with varying pressure. The lower band-edge shifts from 60 THz to 62.58 THz, and the upper band-edge shifts from 62.41 THz to 64.95 THz with varying pressure from 0 MPa to 200 MPa. The change in size of the PBG with varying pressure is negligible. Since both media in the 1DPC are polymers and have almost equal rigidity, therefore their contrast in refractive index does not change much with the pressure, resulting constant PBG.

The transmission spectrum of the $(PS/SiO_2)^{50}$ 1DPC with varying hydrostatic pressure is shown in Fig. 8 (a). The 1DPC acts as a high reflection mirror having reflectivity ~99% for the specific photonic band. The high reflection band of the mirror is exactly matching with its calculated PBG as shown in Fig. 7. The high reflection band-edges of the mirror shift to higher frequency with increasing hydrostatic pressure, whereas the reflection bandwidth remains nearly constant. There is a shifting of ~2.55 THz for both lower and upper band-edge of the mirror. The results show that the mirror can be tuned to the required spectral range in the mid-infrared region of 60–65 THz without affecting its bandwidth by controlling the external applied hydrostatic pressure.

The PS/PMMA 1DPC structure is modified for narrow bandpass filter with operating frequencyω_0 = 61.25 THz as $(PS/PMMA)^{25}Air(PS/PMMA)^{25}$. The width of the air gap (defect layer) corresponding to the operating frequency as per Eq. (14) is 1.23 μm. The calculated transmission of the bandpass filter with varying hydrostatic pressure is shown in Fig. 8(b). The figure shows that the resonant transmission occurs in the centre of the PBG and the operating frequency of the filter shift towards higher frequency with increasing hydrostatic pressure. The operating frequency shifts from 61.25 THz to 63.68 THz by increasing pressure from 0 MPa to 200 MPa. The full width half maximum of the filter does not change much with varying hydrostatic pressure and; consequently, the quality factor Q of the filter remains nearly constant. The calculation shows that PS/PMMA based filter can be tuned to the desired operating frequency within the mid-infrared region of 60–65 THz with fixed Q factor by controlling externally applied hydrostatic pressure.

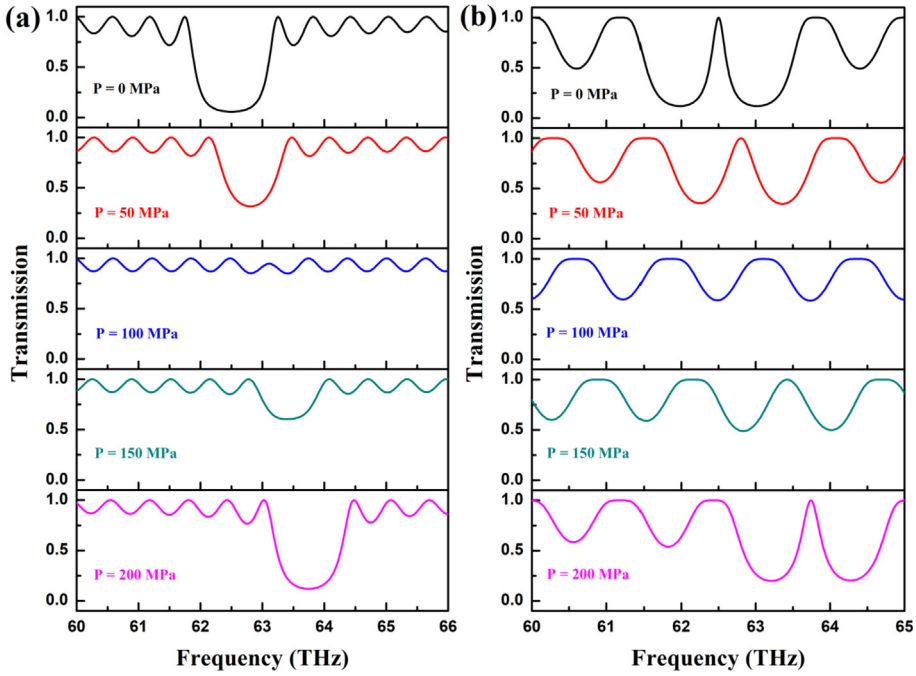

Fig. 6. Transmission spectra of (a) $(PMMA/SiO_2)^{100}$ 1DPC as high reflection mirror, and (b) $(PMMA/SiO_2)^{50}Air(PMMA/SiO_2)^{50}$ 1DPC with defect as narrow bandpass filter with varying hydrostatic pressure P.

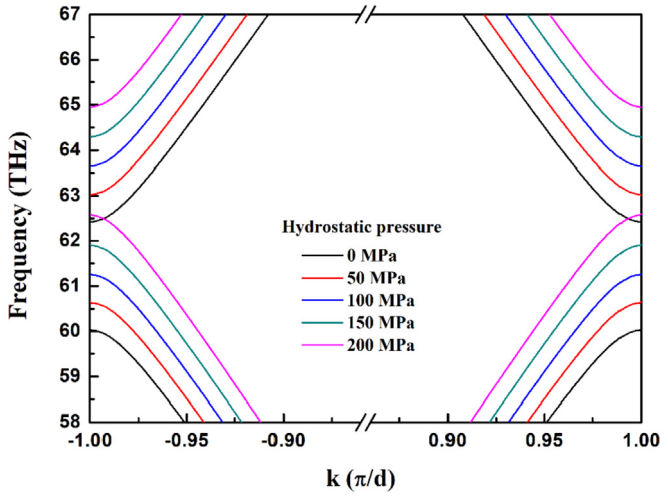

Fig. 7. Photonic band structure of PS/PMMA 1DPC with varying hydrostatic pressure.

Kimura et al. [31] observed blueshift in the transmission spectrum of a distributed Bragg reflector (DBR) filter made of polymer materials under hydrostatic compression. In the present study, the transmission spectrum of all the 1DPC DBR mirrors shifts to higher frequency with increasing pressure. The lower and upper band edges of a DBR mirror are assumed to be the cut-off frequencies above which the reflectivity is ≥ 95% of the reflectivity at the central frequency or mid-band frequency. The bandwidth is simply the difference between the lower and upper band edge frequencies. The ratio of bandwidth to mid-band frequency of a 1DPC is called as band to mid-band ratio. Fig. 9(a) shows the variation of band to mid-band ratio ($\Delta\nu/\nu_c$) of the 1DPC mirrors with applied hydrostatic compressive pressure. The band to mid-band ratio decreases more sharply with increasing pressure in case of PS/SiO_2 1DPC mirror as compared to that of PMMA/PS 1DPC mirror. For $PMMA/SiO_2$ 1DPC mirror, the band to mid-band ratio initially decreases close to zero and again increases with increasing pressure. This shows that $PMMA/SiO_2$ 1DPC can be made as a reflector as well as a transparent medium by tuning the applied hydrostatic pressure, which can be used for mechanically switchable optical devices. Sayginer et al. [51] have fabricated a Fabry-Perot filter $[(TiO_2/SiO_2)^7$ PDMS $(TiO_2/SiO_2)^7]$ with Polydimethylsiloxane (PDMS) as an elastic microcavity layer for mechanical sensing, and they have observed that the cavity peaks shift to longer wavelength and their intensity increases with increasing applied force. The peak of our designed filters shifts to higher frequency or lower wavelength with increasing applied pressure and the shift is more distinct. The shift of operating frequency or defect mode of the 1DPC filters with varying hydrostatic pressure is plotted in Fig. 9(b). The frequency shift is large in case of PMMA/PS 1DPC filter as compared to the other two filters. The PMMA/PS filter has higher pressure sensitivity of 11.96 GHz/MPa, while the pressure sensitivity of PS/SiO_2 and $PMMA/SiO_2$ filters are 6.39 GHz/MPa and 6.16 GHz/MPa, respectively, which are close to each other. The PMMA/PS 1DPC filter is more suitable for hydrostatic pressure sensing application because of its better sensitivity. The polymer based mechanically tunable photonic crystal are likely to have potential applications in tunable optical wave guides and tunable lasers. To examine the pressure sensitivity of the polymer based 1DPC mirrors and filters, an experimental methodology is proposed below.

Optical fibre technology as well as the availability of IR-light sources in the frequency range of 30–150 THz [52] can be used to design an experimental set-up to investigate the tunable optical properties of the photonic devices. Fig. 10 is the schematic of an experimental arrangement to measure the spectral transmission of a 1DPC subject to hydrostatic compression perpendicular to the z-axis of the multilayer. Fibre coupled infrared-light-source is incident on the 1DPC along the z-axis and the transmitted light is collected by an optical fibre coupled spectrophotometer. The required tunable optical properties such as photonic bandgap, defect mode, transmission, etc., of the 1DPC can be obtained by controlling the applied load through the pressure gauge. Selective layer/layers of the 1DPCs can also be compressed for tunable optical properties by modifying the geometry of the press head. This experimental setup can also be used to investigate the mechanical tunabiltiy of 1DPCs other than the simulated polymer based 1DPC mirrors/filters, provided that the 1DPCs are transparent in that spectral region.

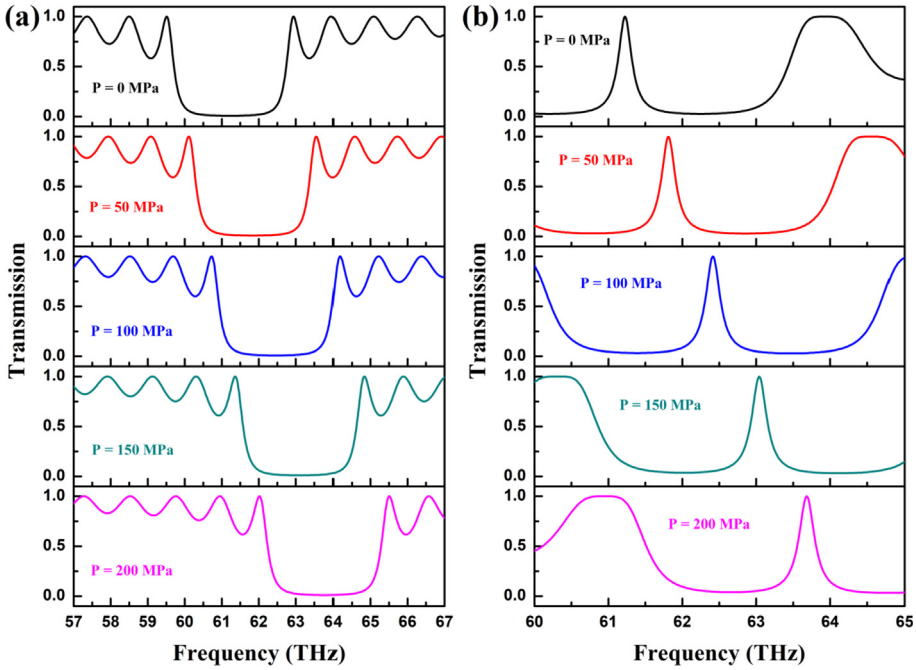

Fig. 8. Transmission spectra of (a) $(PS/PMMA)^{50}$ 1DPC as high reflection mirror, and (b) $(PS/PMMA)^{25}Air(PS/PMMA)^{25}$ 1DPC with defect as narrow bandpass filter with varying hydrostatic pressure P.

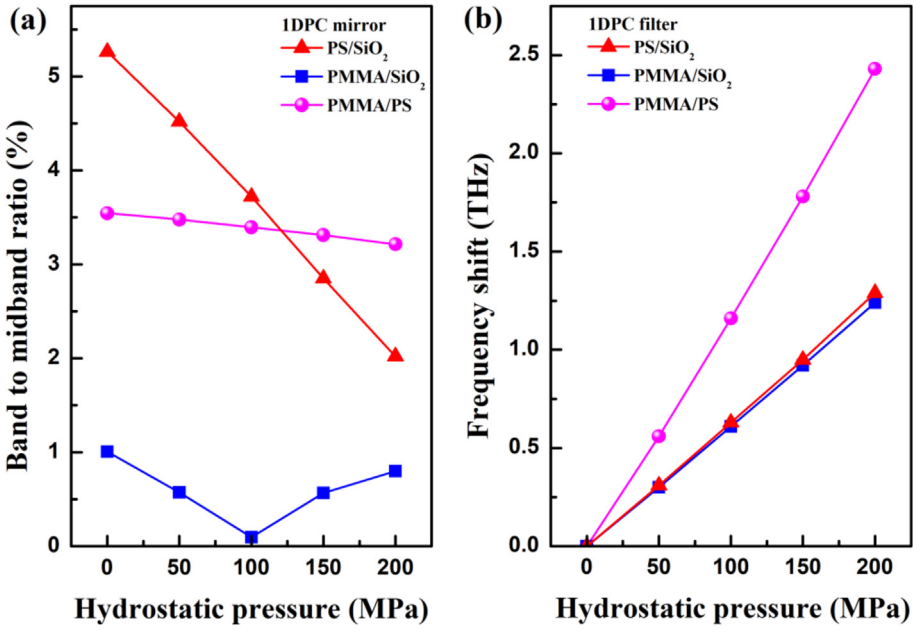

Fig. 9. Pressure dependent (a) band to mid-band ratio of 1DPC mirrors, and (b) frequency shift of the 1DPC filters.

4. Conclusion

We have studied the hydrostatic pressure dependent band structure and spectral transmission of three different combinations of polymer materials based 1DPC mirrors and filters. The elasto-optic behaviour of the polymer materials enables the tuning properties of the 1DPCs. The PBG of the mirrors and the operating frequency of the filters are found shifting towards higher frequency with increasing pressure, which are primarily due to the decreasing refractive index of the polymer materials with increasing pressure. The band to midband ratio of the mirrors and fullwidth half maximum of the filters are tunable under compression. The $PMMA/SiO_2$ 1DPC can be used as a switchable mirror as the transmission of the mirror can be varied from less than 5% to more than 90% by varying hydrostatic pressure. The PMMA/PS 1DPC filter exhibits higher pressure sensitivity and its operating frequency can be tuned to the desired frequency without affecting its quality factor by controlling externally applied pressure. The designs of the polymer based tunable mirrors and filters are simple and adaptable, which will provide many opportunities for photonic devices, and tunable/switchable filters in the mid-infrared region.

Acknowledgements

The authors are grateful to Dr. M. N. Deo, Head, Atomic & Molecular Physics Division for his continuous encouragement and support in carrying out the research.

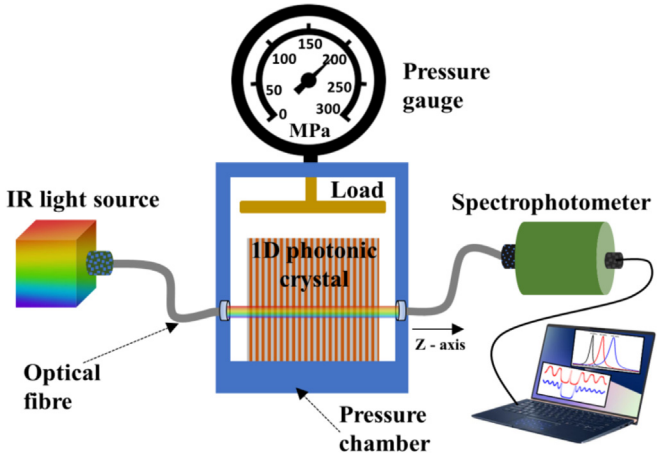

Fig. 10. Experimental setup to measure transmission of a 1DPC under compression.

References

[1] J.D. Joannopoulos, P.R. Villeneuve, S. Fan, Photonic crystals: putting a new twist on light, Nature 386 (1997) 143.
[2] N. Masaya, Manipulating light with strongly modulated photonic crystals, Rep. Prog. Phys. 73 (2010) 096501.
[3] S. Jena, R.B. Tokas, P. Sarkar, J.S. Misal, S. Maidul Haque, K.D. Rao, S. Thakur, N.K. Sahoo, Omnidirectional photonic band gap in magnetron sputtered TiO2/SiO2 one dimensional photonic crystal, Thin Solid Films 599 (2016) 138.
[4] H.-C. Hung, C.-J. Wu, S.-J. Chang, Terahertz temperature-dependent defect mode in a semiconductor-dielectric photonic crystal, J. Appl. Phys. 110 (2011) 093110.
[5] J. Peng, D. Lyu, Y. Qu, W. Wang, T. Sun, M. Yang, Thin films based one-dimensional photonic crystal for refractive index sensing, Optik 158 (2018) 1512.
[6] M. Rahmat, T. Negara, H. Hardhienata, H. Alatas, Real-time optical sensor based on one dimensional photonic crystals with defects, Instrumentation, Communications, Information Technology, and Biomedical Engineering (ICICI-BME), International Conference on, 2009, p. 1 2009.
[7] A. Bouzidi, D. Bria, A. Akjouj, Y. Pennec, B. Djafari-Rouhani, A tiny gas-sensor system based on 1D photonic crystal, J. Phys. D Appl. Phys. 48 (2015) 495102.
[8] A. Bouzidi, B. Bria, F. Falyouni, A. Akjouj, G. Lévêque, M. Azizi, H. Berkhli, A biosensor based on one-dimensional photonic crystal for monitoring blood glycemia, J. Mater. Environ. Sci. 8 (2017) 3892.
[9] K. Busch, S. John, Liquid-crystal photonic-band-gap materials: the tunable electromagnetic vacuum, Phys. Rev. Lett. 83 (1999) 967.
[10] R. Ozaki, T. Matsui, M. Ozaki, K. Yoshino, Electrically color-tunable defect mode lasing in one-dimensional photonic-band-gap system containing liquid crystal, Appl. Phys. Lett. 82 (2003) 3593.
[11] C. Xu, X. Hu, Y. Li, X. Liu, R. Fu, J. Zi, Semiconductor-based tunable photonic crystals by means of an external magnetic field, Phys. Rev. B 68 (2003) 193201.
[12] H. Tian, J. Zi, One-dimensional tunable photonic crystals by means of external magnetic fields, Optic Commun. 252 (2005) 321.
[13] P. a. Halevi, F. Ramos-Mendieta, Tunable photonic crystals with semiconducting constituents, Phys. Rev. Lett. 85 (2000) 1875.
[14] H. Němec, L. Duvillaret, F. Garet, P. Kužel, P. Xavier, J. Richard, D. Rauly, Thermally tunable filter for terahertz range based on a one-dimensional photonic crystal with a defect, J. Appl. Phys. 96 (2004) 4072.
[15] L.E. González, N. Porras-Montenegro, Pressure, temperature and plasma frequency effects on the band structure of a 1D semiconductor photonic crystal, Physica E 44 (2012) 773.
[16] N. Porras-Montenegro, C.A. Duque, Temperature and hydrostatic pressure effects on the photonic band structure of a 2D honeycomb lattice, Physica E 42 (2010) 1865.
[17] H. Fu, H. Tam, L.-Y. Shao, X. Dong, P. Wai, C. Lu, S.K. Khijwania, Pressure sensor realized with polarization-maintaining photonic crystal fiber-based Sagnac interferometer, Appl. Opt. 47 (2008) 2835.
[18] K. Vijaya Shanthi, S. Robinson, Two-dimensional photonic crystal based sensor for pressure sensing, Photonic Sens. 4 (2014) 248.
[19] D. Chen, G. Hu, L. Chen, Dual-core photonic crystal fiber for hydrostatic pressure sensing, IEEE Photonics Technol. Lett. 23 (2011) 1851.
[20] A.Y. Herrera, J.M. Calero, N. Porras-Montenegro, Pressure, temperature, and thickness dependence of transmittance in a 1D superconductor-semiconductor photonic crystal, J. Appl. Phys. 123 (2018) 033101.
[21] F. Segovia-Chaves, H. Vinck-Posada, Tuning of transmittance spectrum in a one-dimensional superconductor-semiconductor photonic crystal, Physica B 543 (2018) 7.
[22] F. Segovia-Chaves, H. Vinck-Posada, Dependence of the defect mode with temperature, pressure and angle of incidence in a 1D semiconductor-superconductor photonic crystal, Physica C 553 (2018) 1.
[23] M.M. Tefelska, M. Chychłowski, A. Czapla, R. Dabrowski, S. Ertman, E. Nowinowski-Kruszelnicki, J. Wójcik, T. Woliński, Hydrostatic Pressure Effects in Photonic Liquid Crystal Fibers, (2008).
[24] C. Wu, H. Fu, K.K. Qureshi, B.-O. Guan, H.-Y. Tam, High-pressure and high-temperature characteristics of a Fabry–Perot interferometer based on photonic crystal fiber, Opt. Lett. 36 (2011) 412.
[25] Z. Liu, M.-L.V. Tse, C. Wu, D. Chen, C. Lu, H.-Y. Tam, Intermodal coupling of supermodes in a twin-core photonic crystal fiber and its application as a pressure sensor, Optic Express 20 (2012) 21749.
[26] D. Turchinovich, A. Kammoun, P. Knobloch, T. Dobbertin, M. Koch, Flexible all-plastic mirrors for the THz range, Appl. Phys. A 74 (2002) 291.
[27] N. Krumbholz, K. Gerlach, F. Rutz, M. Koch, R. Piesiewicz, T. Kürner, D. Mittleman, Omnidirectional terahertz mirrors: a key element for future terahertz communication systems, Appl. Phys. Lett. 88 (2006) 202905.
[28] C. Jansen, S. Wietzke, V. Astley, D.M. Mittleman, M. Koch, Mechanically flexible polymeric compound one-dimensional photonic crystals for terahertz frequencies, Appl. Phys. Lett. 96 (2010) 111108.
[29] D. Scripka, G. LeCroy, C.J. Summers, N.N. Thadhani, Spectral response of multilayer optical structures to dynamic mechanical loading, Appl. Phys. Lett. 106 (2015) 201906.
[30] C. Ghouila-Houri, J.-C. Gerbedoen, R. Viard, A. Talbi, A. Merlen, P. Pernod, L. I. A. L. L. Joint International Laboratory, Design and elaboration of 1D photonic crystal cavity based on highly flexible elastomer thin layer for sensors applications, Procedia Eng. 120 (2015) 744.
[31] M. Kimura, K. Okahara, T. Miyamoto, Tunable multilayer-film distributed-Bragg-reflector filter, J. Appl. Phys. 50 (1979) 1222.
[32] M. Kolle, B. Zheng, N. Gibbons, J.J. Baumberg, U. Steiner, Stretch-tuneable dielectric mirrors and optical microcavities, Optic Express 18 (2010) 4356.
[33] F. Segovia-Chaves, H. Vinck-Posada, Simultaneous effects of the hydrostatic pressure and the angle of incidence on the defect mode of a one-dimensional photonic crystal of GaAs/Ga0.7Al0.3As, Optik 164 (2018) 686.
[34] F. Segovia-Chaves, H. Vinck-Posada, The effect of hydrostatic pressure and temperature on the defect mode in a GaAs/Ga0.7Al0.3As one-dimensional photonic crystal, Optik 159 (2018) 169.
[35] F. Segovia-Chaves, H. Vinck-Posada, Tuning of the defect mode in a 1D superconductor-semiconductor crystal with hydrostatic pressure dependent frequency of the transverse optical phonons, Physica C 556 (2019) 7.
[36] A. Sánchez, S. Orozco, Elasto-optical effect on the band structure of a one-dimensional photonic crystal under hydrostatic pressure, J. Opt. Soc. Am. B 33 (2016) 1406.
[37] M. Nedeljkovic, A. Khokhar, Y. Hu, X. Chen, J.S. Penades, S. Stankovic, H. Chong, D. Thomson, F. Gardes, G. Reed, Silicon photonic devices and platforms for the mid-infrared, Opt. Mater. Express 3 (2013) 1205.
[38] R. Shankar, R. Leijssen, I. Bulu, M. Lončar, Mid-infrared photonic crystal cavities in silicon, Optic Express 19 (2011) 5579.
[39] B. Weng, J. Qiu, Z. Shi, Continuous-wave mid-infrared photonic crystal light emitters at room temperature, Appl. Phys. B 123 (2017) 29.
[40] J. He, S. Chen, H. Huang, B. Chen, X. Xiao, J. Lin, Q. Chen, Novel anisotropic janus composite particles based on urushiol-erbium chelate polymer/polystyrene, Soft Mater. 13 (2015) 237.
[41] G. Duan, C. Zhang, A. Li, X. Yang, L. Lu, X. Wang, Preparation and characterization of mesoporous zirconia made by using a poly (methyl methacrylate) template, Nanoscale Res. Lett. 3 (2008) 118.
[42] B. Shokri, M.A. Firouzjah, S. Hosseini, FTIR analysis of silicon dioxide thin film deposited by metal organic-based PECVD, Proceedings of 19th International Symposium on Plasma Chemistry Society, 2009, p. 2631 Bochum, Germany.
[43] S.K. Srivastava, S. Ojha, Broadband optical reflector based on Si/SiO2 one-dimensional graded photonic crystal structure, J. Mod. Opt. 56 (2009) 33.
[44] A. Mishra, S.K. Awasthi, S.K. Srivastava, U. Malaviya, S.P. Ojha, Tunable and omnidirectional filters based on one-dimensional photonic crystals composed of single-negative materials, J. Opt. Soc. Am. B 28 (2011) 1416.
[45] D. Lusk, I. Abdulhalim, F. Placido, Omnidirectional reflection from Fibonacci quasi-periodic one-dimensional photonic crystal, Optic Commun. 198 (2001) 273.
[46] T.S. Narasimhamurty, Photoelastic and Electro-Optic Properties of Crystals, Springer Science & Business Media, 2012.
[47] A. Sánchez, A. Porta, S. Orozco, Photonic band-gap and defect modes of a one-dimensional photonic crystal under localized compression, J. Appl. Phys. 121 (2017) 173101.
[48] J. Lekner, Omnidirectional reflection by multilayer dielectric mirrors, J. Opt. A Pure Appl. Opt. 2 (2000) 349.
[49] H.A. Macleod, H.A. Macleod, Thin-film Optical Filters, CRC press, 2010.
[50] R. Hikmet, H. Kemperman, Electrically switchable mirrors and optical components made from liquid-crystal gels, Nature 392 (1998) 476.
[51] O. Sayginer, A. Chiasera, L. Zur, S. Varas, L.T.N. Tran, C. Armellini, M. Ferrari, O.S. Bursi, Fabrication, modelling and assessment of hybrid 1-D elastic Fabry Perot microcavity for mechanical sensing applications, Ceram. Int. 45 (2019) 7785.
[52] M. Hassan, X. Tan, E. Welle, I. Ilev, Fiber-optic Fourier transform infrared spectroscopy for remote label-free sensing of medical device surface contamination, Rev. Sci. Instrum. 84 (2013) 053101.